UNIVERSITY OF CALIFORNIA SAN DIEGO

SPATIAL VARIABILITY OF ANTARCTIC BOTTOM WATER IN THE AUSTRALIAN ANTARCTIC BASIN FROM 2018-2020 CAPTURED BY DEEP ARGO

A thesis submitted in partial satisfaction of the
requirements for the degree Master of Science

in

Earth Sciences

by

George Thomas

Committee in charge:

Professor Sarah G. Purkey, Chair
Professor Mark Merrifield
Professor Dean Roemmich

2020

The thesis of George Thomas is approved, and it is acceptable in quality and form for publication on microfilm and electronically:

_____

_____

_____

Chair

University of California San Diego

2020

TABLE OF CONTENTS

LIST OF FIGURES

LIST OF TABLES

ACKNOWLEDGEMENTS

We would like to thank the crews of the research vessels that have provided this data, as well as those that work with the Argo program to prepare the data for study. Argo data are made freely available by the international Argo Project office (https://www.usgodae.org/argo/argo.html).

Shipboard repeat hydrographic data were collected and made publicly available by the International Global Ship-based Hydrographic Investigations Program (GO-SHIP; http://www.go-ship.org/ , http://cchdo.ucsd.edu).

ETOPO1 (doi:10.7289/V5C8276M) bathymetry data is also made available for the public by the National Center for Environmental Information (NCEI; https://www.ngdc.noaa.gov/mgg/global/).

We would like to thank Paul Chamberlain, Esmee Van Wijk, Luke Wallace, John Gilson, Mark Merrifield and Nathalie Zilberman for providing valuable advice, counsel and guidance. SIO's Deep Argo floats as well as the work of SGP and GJT were supported by NOAA Grant NA15OAR4320071.

AF and SRR were supported in part by the Australian Government's Department of Industry, Innovation and Science, through the Antarctic Science Collaboration Initiative program; by the Centre for Southern Hemisphere Oceans Research, a partnership between CSIRO and the Qingdao National Laboratory for Marine Science and Technology (QNLM); and by the Earth Systems and Climate Change Hub of Australia's National Environmental Science Program.

This paper was co-authored with Purkey, Sarah G., Roemmich, Dean, Foppert, Annie, and Rintoul, Stephen R. The thesis author was the primary author of this paper.

ABSTRACT OF THESIS

SPATIAL VARIABILITY OF ANTARCTIC BOTTOM WATER IN THE AUSTRALIAN ANTARCTIC BASIN FROM 2018-2020 CAPTURED BY DEEP ARGO

by

George Thomas

Master of Science in Earth Sciences

University of California San Diego, 2020

Dr. Sarah G. Purkey, Chair

There are two varieties of Antarctic Bottom Water present in the Australian Antarctic Basin (AAB): locally-produced Adélie Land Bottom Water (ALBW) and distantly-produced Ross Sea Bottom Water (RSBW). Between 2014 and 2018, RSBW has rebounded from a multi-decade freshening trend, with implications for the strength and properties of the bottom limb of the Meridional Overturning Circulation. The return of the salty RSBW to the AAB is revealed by six Deep Argo floats that have occupied the region from January of 2018 to March of 2020. The floats depict a zonal variation in temperature and salinity in the bottom waters of the

AAB, driven by the inflow of RSBW. A simple Optimum Multiparameter Analysis based on potential temperature and salinity gives a sense of scale to the composition of the bottom waters, which are nearly 80% the new, salty RSBW in the south-east corner of the basin by 2019, and generally less than 40% to the west closer to the ALBW outflow region and the abyssal plain.

Chapter 1

Introduction and Background

1.1 Antarctic Bottom Water

Over the past three decades Antarctic Bottom Water (AABW) has played a crucial role in mitigating the increase of anthropogenic atmospheric warming through the sequestration of heat into the abyssal (greater than 4,000 m depth) ocean. Decadal occupations of hydrographic sections gridding the deep ocean conducted by the Global Ocean Ship-based Hydrographic Investigations Program (GO-SHIP; Talley et al., 2016) have shown that the abyssal ocean has warmed significantly throughout the globe (Aoki et al., 2017; Desbruyeres et al., 2016; Johnson et al., 2019; Kobayashi, 2018; Kouketsu et al., 2011; Purkey & Johnson, 2010). This warming is associated with a decrease in AABW volume (Purkey & Johnson, 2012) possibly connected to freshening of AABW throughout the Indo-Pacific sector of the Southern Ocean (e.g., Menezes et al. 2017; Purkey & Johnson, 2013, 2012; Rintoul, 2007; van Wijk & Rintoul, 2014). High resolution models have shown a similar climate signal of abyssal warming driven by anthropogenic forcing near Antarctica (Boe et al., 2009; Bryan et al., 2014; Newsom et al., 2016).

AABW forms in distinct regions on the Antarctic coast (Orsi et al., 1999) that possess certain shelf conditions, including large coastal polynyas, brine rejection due to creation of sea ice, and strong air-sea interaction (Williams et al., 2008). In each region, bottom water originates from dense shelf water (DSW) sinking down the continental slope and entraining local

water masses. In most regions, bottom water is driven westward by the Antarctic Slope Current and nearshore easterly winds (Stewart et al., 2019). The various sources of AABW supply the dense water masses that sink and ventilate the deep ocean basins worldwide (e.g. Johnson, 2008; Rintoul, 1998). There they feed the bottom limb of the Meridional Overturning Circulation (MOC; Ganachaud & Wunsch, 2000; Lumpkin & Speer, 2007; Sloyan & Rintoul, 2001; Talley, 2003) and fill the bottom half of the global ocean (Johnson, 2008).

1.2 Sources of Antarctic Bottom Water

Two recurrent areas of AABW formation are the Adélie and George V Land (AGVL) coast and the Ross Sea, both of which supply bottom water to the Australian Antarctic Basin (AAB; Rintoul, 2007, 1998; van Wijk & Rintoul, 2014) before mixing in the Antarctic Circumpolar Current (ACC) and eventually being exported into the Indian and Pacific Oceans. Each region produces bottom water with unique characteristics, and as such are named Adélie Land Bottom Water (ALBW) and Ross Sea Bottom Water (RSBW). RSBW and ALBW temperature and salinity properties are distinct, owing to differences in the production processes of the two water masses. The RSBW production regime is governed by a wide continental shelf and a land boundary that limits westward outflow of shelf water while its salinity is increased by brine rejection processes. This historically produces the saltiest variety of AABW, which flows out of the western side of the Ross Sea, around Cape Adare, and into the AAB (Shimada et al., 2012; van Wijk & Rintoul, 2014). Conversely, because the ALBW formation region lacks these properties, it relies on heavy brine rejection in a coastal polynya over the Adélie Depression, which is located in the lee of the Mertz Glacier Tongue (Figure 1; Bindoff et al., 2000a, 2001;

Rintoul, 1998; Williams et al., 2008). Maintenance of this polynya is likely aided by especially strong regional katabatic winds (Wendler et al., 1997), atmospheric forcing from storm events (Massom et al., 2001), and high rates of Modified Circumpolar Deep Water (MCDW) intrusion (Williams et al., 2008).

1.3 Variability in Antarctic Bottom Water Properties

Observations within and near formation regions have shown large variations in the properties of RSBW and ALBW since the 1960s (Figure 2a; e.g. Aoki et al., 2005; Jacobs & Giulivi, 2010; Rintoul 2007; Swift & Orsi, 2012; van Wijk & Rintoul, 2014). The calving of the Mertz Glacier Tongue in 2010 altered ALBW composition on an interannual time scale, owing to changes in factors such as sea ice production (Snow et al., 2018) and input of freshwater from continental melt (Aoki et al., 2017). High Salinity Shelf Water (HSSW) in the Ross Sea, a precursor to RSBW, freshened at a rate near 0.03 dec^{-1} between the 1960s and 2000s (Jacobs et al., 2002; Jacobs & Giulivi, 2010), but rebounded very quickly in the period 2014-2018 (Castagno et al., 2019). The fresher shelf water prior to 2014 created a fresher variety of RSBW and affected the quantity, circulation and properties found along the outflow path of RSBW and ALBW, which was observed as a deep freshening or warming on abyssal pressure surfaces throughout the Indo-Pacific Southern Ocean and as far north as the Southwest Pacific Basin (Aoki et al., 2005; Johnson, 2008; Menezes et al., 2017; Purkey et al., 2019; Shimada et al., 2012; Swift & Orsi, 2012; Rintoul, 2007; van Wijk & Rintoul, 2014). This earlier freshening trend coincided with a decrease in the volume of dense water that is produced (Purkey & Johnson, 2012).

1.4 Deep Argo

Despite the production of this deep, cold water being a significant element of the earth's Global Thermohaline Circulation (Lumpkin & Speer, 2007; Talley, 2003), in situ observations of this annual cycle are relatively sparse, with the majority of data used to study the region concentrated in the austral summer months due to problems posed by wintertime ship observations. Beginning in 2014, the international oceanic observation program Argo began deploying autonomous Deep Argo floats capable of sampling temperature, salinity and pressure down to a depth of 6000 m. This relatively new Deep Argo Program represents a significant step toward tracking changes in the abyssal ocean, since Core Argo floats are only capable of profiling down to 2000 m. Data from these floats will provide far greater spatial and temporal resolution of abyssal processes than was previously possible from repeat hydrographic GO-SHIP sections or more traditional Argo floats (Johnson et al., 2019; Kobayashi, 2018; Roemmich et al., 2019).

1.5 Research Objectives for This Study

Here we describe the properties and sources of AABW found in the southern AAB and quantify the return of salty RSBW spreading into the AAB from the east, as observed by Deep Argo floats from January of 2018 to March of 2020. Furthermore, we assess the viability of Deep Argo in such a hostile region and demonstrate the value these data provide. In the next section, we will describe the Deep Argo and GO-SHIP data, as well as the analysis methods we used to produce our results. These results will be presented in section 3, and in section 4 we will discuss and explore their meaning.

Our research objectives:

(1) Assess the performance of Deep Argo floats in this region and determine if and how they improve observation.

(2) Capture the return of salty, post-2014 Ross Sea Bottom Water to the Australian Antarctic Basin.

(3) Make a preliminary calculation of the amount of salty Ross Sea Bottom Water in the region.

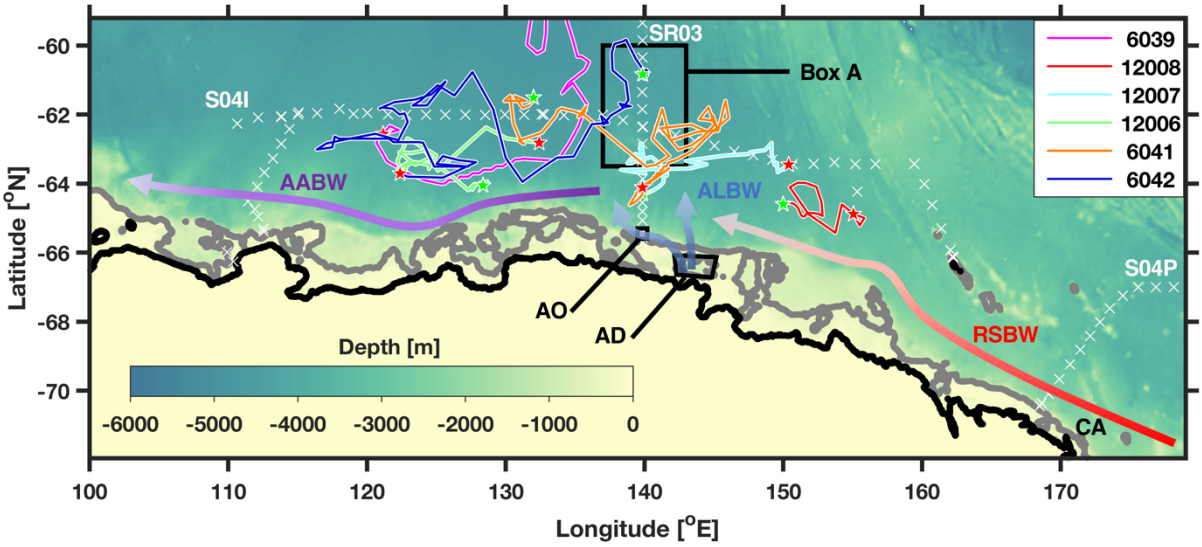

Figure 1: Paths of six Deep Argo floats (colors) are shown in relation to bathymetry from ETOPO1 (color bar; doi:10.7289/V5C8276M). The deployment position for each float is marked by a green star, and the most recent profile position as of April 1st, 2020 is marked by a red star. CTD profile locations from the most recent occupations of the three previously mentioned GO-SHIP sections are marked by white x's and labeled. Additionally, the 0 and 500 m depth isobaths (thick black and grey lines, respectively), and locations such as the ALBW Outflow (AO) region, Adélie Depression (AD), and Cape Adare (CA) are shown. Box A, used in Figure 2a, is also shown. Finally, general flow paths of Adélie Land Bottom Water (ALBW), Ross Sea Bottom Water (RSBW), and the mix of the two here referred to simply as Antarctic Bottom Water (AABW), in the region are represented by blue, red, and purple arrows, respectively.

Chapter 2

Data and Methods

2.1 Data

Data from two observational platforms were analyzed in this study: data from autonomous Deep SOLO floats and from shipboard hydrography sections occupied on a decadal basis.

2.1.1 Deep Argo Floats

2.1.1.1 *Floats Deployed in the Australian Antarctic Basin*

Between January 2018 and March 2019, 8 Deep SOLO floats were deployed in the AAB with the purpose of providing a preliminary look at AABW production in this region. The Deep SOLOs, one of 4 models of Deep Argo floats, profile from the surface to within 3 m of the bottom or to a maximum pressure of 6000 dbar, measuring temperature, salinity, and pressure at user-prescribed intervals between the sea surface and bottom (Roemmich et al., 2019). The Deep SOLOs are outfitted with a wire for passive bottom detection as well as an ice sensing algorithm (Klatt et al., 2007; Roemmich et al., 2019). Five floats fabricated by Scripps Institution of Oceanography (SIO) were deployed in January-February of 2018 from the *R/V Investigator*. Three additional floats of the MRV Deep SOLO model, provided by the

Commonwealth Scientific and Industrial Research Organization (CSIRO), were deployed in January-March of 2019 from the *R/V Kaiyo Maru* (Figure 1). The six floats nearest the continental shelf are the focus of this paper (Figure 1).

2.1.1.2 *Corrections and Alterations to Float Data*

All Deep SOLO and MRV Deep SOLO floats carry Seabird SBE-61 CTD (Conductivity, Temperature, Depth) sensors, with accuracy goals of ± 0.001°C, ± 0.002, and ± 3 dbar for temperature, salinity and pressure, respectively. All Deep Argo data were obtained from the Argo Global Data Assembly Center (GDAC) on April 1st, 2020 (https://doi.org/10.17882/42182). A correction for the conductivity cell compressibility coefficient (cpcor) is applied to all floats from the default value of -9.57 x 10^{-8} $dbar^{-1}$ to -11.66 x 10^{-8} $dbar^{-1}$ (Murphy & Martini, 2018; Roemmich et al., 2019). In addition, any salinity spikes (defined as a change greater than 0.01 between sampling bins) were removed, including very fresh (negative 1-10) spikes found in the bottom 1-2 bins of some profiles, possibly owing to low conductivity driven by increased sediment close to the bottom. Potential temperature (θ) and depth are derived from the CTD profile.

No floats had a detectable drift in salinity. Using all profiles taken in water deeper than 3000 m where the θ-Salinity relationship is relatively tight away from the continental slope, all floats show a scatter within ± 0.004 of the mean salinity along the 0.5°C isotherm with time, with most falling within the accuracy goal of ± 0.002 over the time considered here. In addition, all float and co-located GO-SHIP salinity profiles within 220 km agreed within the ± 0.002 in the isotherm range between 0 and 1°C.

Due to the lack of location data for winter profiles taken under sea ice, the locations of more than a quarter of the total float profiles are unknown. Using maximum recorded depth as a constraint, we have developed a novel, simple method of determining revised float paths (Appendix). In order to serve as an example, only the winter 2018 profiles of float 6042 were altered (Figure A1).

2.1.2 Shipboard Hydrography Sections

Multiple occupations of high quality, full depth, ship based CTD profiles collected along three GO-SHIP hydrographic track lines (https://cchdo.ucsd.edu/) are also considered here, including SR03, a meridional line along 140°E, occupied 10 times between 1991 and 2018, S04I, a zonal line along 62°S, occupied 3 times between 1995 and 2013, and S04P, which starts along the continental shelf near Cape Adare and heads northeast before following latitude 67°S, occupied 3 times between 1992 and 2018 (Figure 1). All GO-SHIP sections provide high quality CTD data measured on decadal timescales along set paths throughout the ocean. Vertical sections are measured to within 10-20 m of the bottom. The CTD salinity data are all calibrated to bottle salinities that are referenced to the International Association for the Physical Sciences of the Oceans (IAPSO) standard seawater. The shipboard CTD sensor has accuracies of ± 0.002 for salinity, ± 0.002°C for temperature, and ± 3 dbar for pressure (Joyce, 1991). Only data with good quality control flags were used.

2.2 Methods

To provide an estimate of the fraction of the recent, salty variety of RSBW present in the region, a simple version of an Optimum Multiparameter (OMP) analysis was performed, based

solely on two conservative tracers: θ and salinity (Tomczak & Large, 1989). An OMP analysis uses a system of linear equations to determine what fraction of different water masses are present. For the purposes of this paper, it serves as a back-of-the-envelope calculation to determine the distribution of ALBW versus the new, salty RSBW along the bottom of the near-shelf AAB.

2.2.1 Optimum Multiparameter Analysis

A system of three linear equations with a non-negative constraint was solved at each depth of each profile (Equation 1).

$$x_1\theta_{ALBW} + x_2\theta_{RSBW} + x_3\theta_{CDW} = \theta_{obs} \quad (1a)$$
$$x_1S_{ALBW} + x_2S_{RSBW} + x_3S_{CDW} = S_{obs} \quad (1b)$$
$$x_1 + x_2 + x_3 = 1 \quad (1c)$$

Equations 1a and 1b conserve potential temperature (θ) and salinity (S) and 1c conserves mass. The fraction of ALBW, RSBW and CDW for each in-situ observation (obs) of θ and S is given by x_1, x_2, and x_3, respectively.

2.2.2 Water Mass Endmembers

The ALBW, RSBW and CDW endmember temperature and salinity (Equation 1a-b, $\theta/S_{ALBW,RSBW,CDW}$) are estimated from 2018 GO-SHIP cruises. The RSBW endmember (Figure 2b,c; red asterisk) properties of 34.7040 and -0.5994°C (Table 1) are taken to be the average of the bottom properties at the three southernmost positions of the 2018 S04P occupation that are not on the continental slope (Figure 2b, grey). These profiles are roughly between 69.6 and 70.2°S, with a maximum depth range of ~2700 to ~2800 m (Figure 1). These profiles were

chosen because they display a clear RSBW signature along the bottom. Note, here we are choosing the RSBW endmember to be RSBW in 2018, representing the recent post-2014 shift toward salty RSBW. Therefore, any fraction of RSBW discussed hereafter represents the fraction of post-2014 RSBW. The ALBW endmember (Figure 2b,c; blue asterisk) properties of 34.6193 and -0.6316°C (Table 1) are taken to be the average of the bottom values from the four SR03 profiles, sampled in 2018, within the ALBW outflow region, which we've defined to be the continental slope between 65.3 and 65.6°S. The maximum depth of these profiles ranges from ~800 to ~2400 m. The southernmost profile was excluded because it only extends to a depth of less than 300 m. The CDW endmember (Figure 2b,c; green asterisk) properties of 34.7334 and 1.8308°C (Table 1) were defined from the position in θ-S space of the salinity maximum.

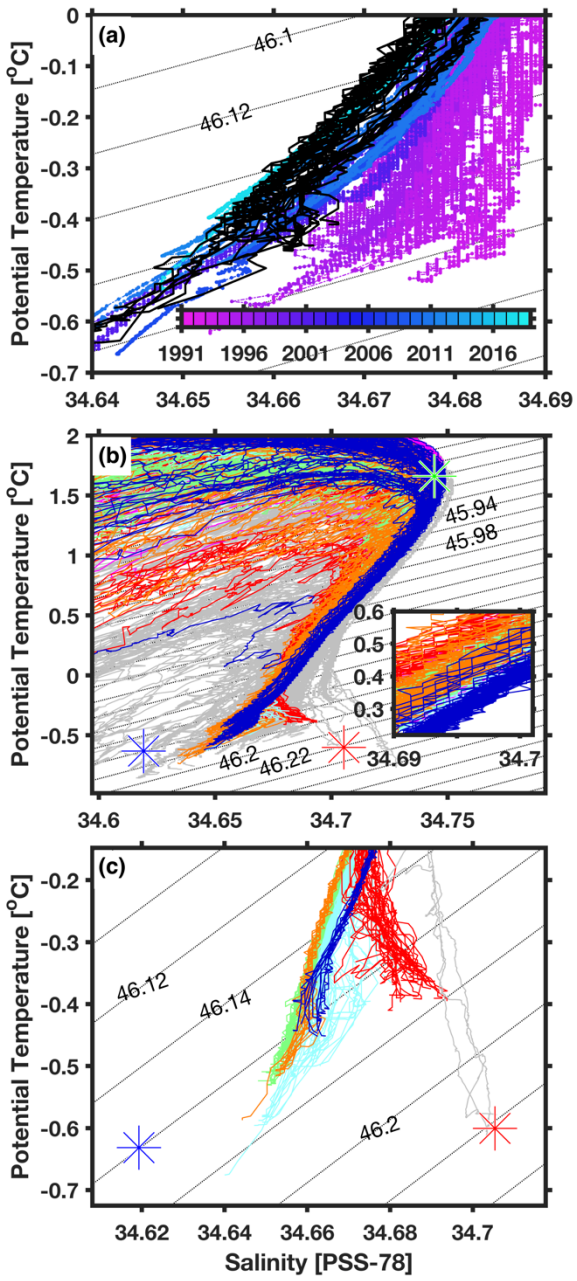

Figure 2: (a) *θ-S* profiles from all occupations (color bar) of SR03 and S04I within Box A (Figure 1) with float profiles (black) from the region.
(b) All float profiles (see Figure 1 color legend) with all years of the GO-SHIP CTD profiles shown in Figure 1 (grey).
(c) A zoomed in view of (b), showing only profiles of floats 12006, 12007, 12008, cycles 19-30 of float 6042, and cycles 261-276 of float 6041. All subplots show σ_4 contours (black dotted) and the RSBW, ALBW and CDW endmembers (Table 1) represented by red, blue and green asterisks, respectively.

Table 1: Endmember θ-S properties for Adélie Land Bottom Water (ALBW), new salty Ross Sea Bottom Water (RSBW), and Circumpolar Deep Water (CDW) defined from GO-SHIP profiles (see text).

	ALBW	RSBW	CDW
θ (°C)	-0.6316	-0.5994	1.8308
Salinity (PSS-78)	34.6193	34.7040	34.7334

Chapter 3

Results

The six Deep Argo floats measured the spatial distribution of bottom properties in the southeastern AAB, providing insight into the general flow paths of ALBW and RSBW into the region (Figure 1; blue and red arrows, respectively). The floats spanned a zonal distance of roughly 2300 km between 115 and 160°E and between 60°S and the Antarctic continental slope (Figure 1). There was no significant pattern of zonal movement, with three floats drifting east-to-west and three flowing west-to-east. Float parking depth mostly ranged from 0 to 600 dbar off the bottom, except for floats 12006 and 12007, which mostly parked at 2500 to 3000 dbar during the study period. During the winter of 2018, floats 6041 and 6042 were under ice from August to November. In the winter of 2019, the floats disappeared under ice any time from May-July and returned in December or January.

3.1 Decadal Freshening Trends

Observations between 1991 and 2018 from shipboard CTD measurements along GO-SHIP tracks SR03 and S04I show the temporal variability in bottom properties observed in recent decades over the abyssal plain and on the continental slope (Figure 2a). This variability reflects changes in both local varieties of AABW and is consistent with previous findings (e.g. Roemmich et al., 2019; Aoki et al., 2005; Johnson, 2008).

The southern end of SR03 between 60 and 64.5°S is located downstream from the ALBW formation region, and shows the variations in both ALBW and RSBW between 1991 and

2018 (Figure 2a). Here, RSBW sits above ALBW and is seen as a salty tail in the θ-S curve around -0.45 C in most years (Figure 1, Box A; Figure 2a). Along -0.4°C, a gradual progression towards fresher conditions is observed, freshening from 34.68 in 1991 to 34.65 in 2011, consistent with the arrival of RSBW from the 1980s-2010s traveling west from the Ross shelf to 140°E. The 2018 SR03 occupation reveals a slight rebound of 0.01, indicating that the salty RSBW that began in 2014 (Castagno et al., 2019) has reached 140°E (Figure 2a).

Below RSBW, the colder, fresher ALBW is seen occupying the bottom 100-400 m of the water column in quantities that vary between different years (Figure 2a). Within Box A, less ALBW was observed in the summers of 1993-1995, 2008 and 2018 as well as the winter of 1995 with only a thin (<100 m) layer of water colder than -0.5°C observed along the section. A much thicker, colder layer around 350 m thick was observed in the winter of 1996 and the summers of 2001 and 2011 along the occupations on the slope and within the deep (>4000 m) abyssal plain with temperatures as low as -0.7°C (Figure 2a).

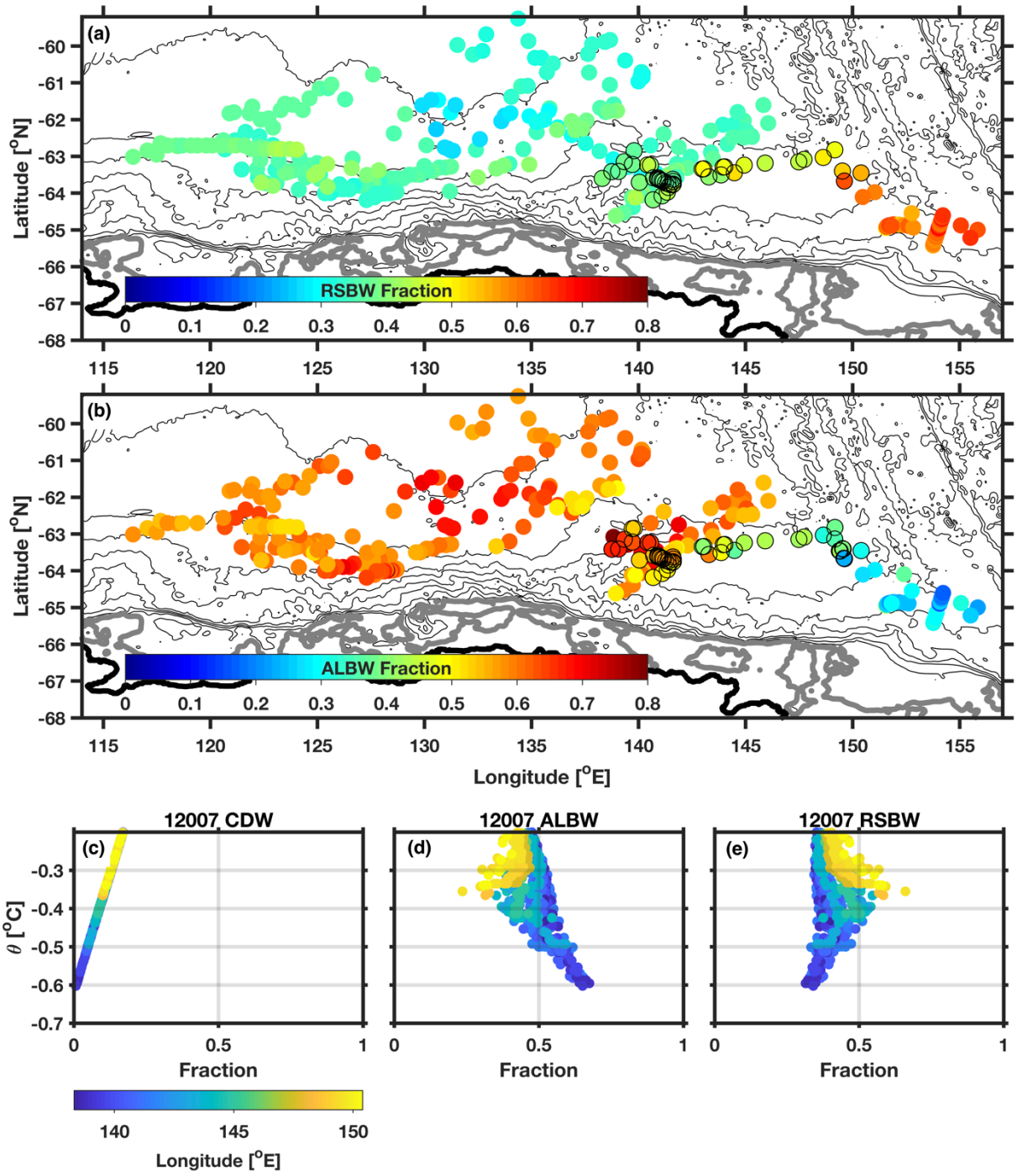

Figure 3: (a) The average fraction of new, salty RSBW between the -0.3 and -0.5°C isotherms (color bar) over 500 m bathymetry contours from ETOPO1 with the 0 and 500 m depth isobaths (thick black and grey lines, respectively) emphasized. The profiles of float 12007 are circled in black. (b) Same as (a) but of the average fraction of ALBW within 200 m of the bottom (color bar). (c-e) The results of the OMP analysis for float 12007 are shown, with each profile colored by its longitude to display the zonal gradient (color bar). They depict the distribution of CDW (c), ALBW (d), and RSBW (e) against θ in each profile.

3.2 Return of Salty Ross Sea Bottom Water

3.2.1 Eastern Floats

The Deep Argo float data map the spatial extent of the return of higher salinity RSBW in the basin in 2018/2019 (Figure 2c, 3). The most eastern float, located in the southeast corner of the basin at ~150E, captured the youngest RSBW in the basin that flows in from the East around Cape Adare (Figure 1; float 12008, red). The February 2018 occupation of the 150°E line showed the deep waters here had warmed by 0.1°C and increased salinity by 0.03 since the last occupation in 2011, with no noticeable (<2 μmol/kg) change in oxygen. The floats also found a 0.04 salty tail at the end of its θ-S curves in the densest water between 46.16 and 45.18 kg/m^3, which differs compared to waters of similar density further east (Figure 2c; float 12008, red). The furthest east profile at 155.8°E is coincidental in θ-S space with profiles measured along S04P in 2018 (Figure 2c; grey) at 45.18 kg/m^3 and it is as salty as bottom water found in the basin in 1991. The OMP analysis supports a strong presence of RSBW in the profiles of 12008, indicating that it is composed of up to 80% RSBW (Figure 3a).

3.2.2 Central Floats

The presence and fraction of new salty RSBW in the study area has a large zonal variation. In the more central floats (Figure 2c; such as float 12007, light blue, and 6041, orange), the salty kink that indicates the presence of new, salty RSBW appears slightly higher in the water column, displaced off the bottom by the denser, colder, and fresher ALBW produced at 142-145°E (Figure 1; AD box). Profiles 19-30 of 6042 at 136-138°E (Figure 2c; dark blue) display this higher bottom salinity, but subsequent profiles taken as the float moved westward do not. The zonal gradient in the recent, salty RSBW along the bottom is clearest in these central floats, which show a relationship between longitude and RSBW fraction in the OMP analysis

(Figure 3c-e). The real variation occurs below the σ_4 potential density surface of 46.1 kg/m^3, which for the profiles of 12007 corresponds to a mean depth of about 3050 m, roughly 500 m off the bottom. From this it is revealed that as the float moved from west to east, it began to record a higher fraction of RSBW at the bottom (Figure 3e).

3.2.3 Western Floats

Farther west still, the influence of recent, salty RSBW is weaker, indicating the greater relative presence of ALBW or older varieties of RSBW in this area. All floats west of 135°E lack the salty kinks or tails that are present in the other floats. In this region, the RSBW fraction is less than 40% along the bottom with slightly higher fractions to the south along the continental slope and lower fractions in the deeper parts of the basin to the north (Figure 3).

3.3 Sensitivity of Optimum Multiparameter Analysis to Endmember Definitions

Though the results of the simple OMP analysis are reliant on the definitions we prescribed for the endmembers, we found that changing the θ values did not greatly affect the results for our purposes. Changing θ for any endmember by ± 0.1°C caused less than a 6% change in the RSBW fraction found at the bottom of a float profile. However, the fraction of RSBW vs ALBW is much more sensitive to the salinity of the endmembers, which are changing in time (Castagno et al., 2019; Jacobs & Giulivi, 2010). Salinity changes of 0.01 to the ALBW and CDW endmembers result in changes to the bottom RSBW fraction on the order of 5%. The fraction is most sensitive to changes in salinity of the RSBW endmember, for which ± 0.01 results in a change to the fraction on the order of 10%.

Chapter 4
Discussion

4.1 Return of Salty Ross Sea Bottom Water

The return of salty RSBW to the AAB in 2018-2020 can be traced with Deep Argo floats. The high salinity bottom water is seen as a salty tail in θ-S curves from float profiles taken in the eastern basin, where RSBW enters the basin and is found at the bottom. It is also seen as a kink in θ-S curves to the west sitting above ALBW (Figure 2c).

4.2 Quantifying the Return

The return of salty RSBW can be quantified using a simple OMP analysis, which finds that the bottom water documented by the float profiles furthest to the east has the greatest fraction of new RSBW at the bottom, over 50% (Figure 3a). It also finds that the fraction decreases moving west and north across the study region along the -0.5°C isotherm (Figure 3a). These θ-S profiles tell the story of dense, new ALBW flowing off the continental shelf and under the lighter and better mixed RSBW coming from the east between 2018-2020 (Figure 2b, c). The OMP analysis agrees with this variability along the bottom, and displays the signal of a zonal gradient in the amount of ALBW at depth (Figure 3b). This work shows it is possible to use the new, salty RSBW as a tracer to examine the flow of RSBW into the AAB at a greater temporal and spatial resolution than ever before.

4.3 Changes in Adélie Land Bottom Water

The northward extent of ALBW in 2018-2020 along 140°E was less than the previous occupations had observed (Figure 2a). The decreased presence of ALBW lowers isotherms, causing warming on isobars and resulting in the mean temperature from SR03 profiles below 1000 m and within Box A to be 0.07°C higher than the mean measured on all SR03 occupations between 1991 and 2018.

4.4 The Role of Floats in the Australian Antarctic Basin

While previous studies have been able to show the return of salty RSBW in the Ross Sea (Castagno et al., 2019), here we quantify it in the AAB using the new Deep Argo observational platform. These floats will provide greater spatial and temporal resolution of changes to AABW occurring on seasonal to decadal timescales, allowing the scientific community to better monitor the variability of AABW in this region. While several issues with the float data remain unanswered, including how to determine the location of float profiles taken during winter, all 6 of the Deep Argo floats deployed in the southern AAB have performed remarkably well despite the harsh conditions. No floats showed salinity drift or were lost during the first two under-ice winters. With more years of data, the temporal and spatial variability in AABW properties within the AAB will be monitored in greater detail. The floats will also serve to bridge the gap between shipboard CTD occupations, allowing for better estimates of variation on longer timescales, such as decadal freshening and warming rates (e.g. Johnson et al., 2019).

4.5 Outlook for Deep Argo

Outside of the AAB, expansion of the Deep Argo Program past its existing pilot arrays will reveal other changes in the abyssal ocean around the world. As Core Argo has drastically advanced our understanding of the upper ocean, Deep Argo is sure to reveal new secrets about the lesser known abyssal waters of the deep ocean.

This paper was co-authored with Purkey, Sarah G., Roemmich, Dean, Foppert, Annie, and Rintoul, Stephen R. The thesis author was the primary author of this paper.

Appendix

A.1 Under Ice Positions

Between deployment and April 1, 2020, the six floats spent more than a fourth of their profiles under sea ice, unable to return to the surface and record GPS fixes of the profile locations. The standard Argo procedure in this event is to linearly interpolate the position for each profile from the last known GPS fix to the next (Scanderbeg et al., 2019). However, we found that this method did not align with the depth, temperature or salinity values found in the floats, particularly in 6042 where the recorded values suggest that the float moved very close to the continental shelf (Figure A1a).

To better put the bottom water properties in context of the processes occurring in the region, new float positions were needed. As of April 2020, there is no widely-accepted procedure for re-assigning profile locations, though bathymetry-constrained float locations are a subject of current research (Wallace et al., 2020). Fortunately, the maximum depth recorded by each profile gives an indication of its location in a near-shelf environment with variable bathymetry.

To test this method, the 2018 winter profiles of float 6042 are used as an example. In order to get a better idea of where the floats moved, we kept the interpolated longitudinal values of each profile and chose latitude values where the maximum depth reached by the float agreed with ETOPO-1 bathymetry within 10 m (Figure A1b). The one exception to this is cycle 35, where the longitude was changed slightly from 128.8 to 129.1°E to match float maximum depth to bathymetry most easily. This process creates expected float paths that align much closer with the temperature and salinity values, showing changes in water properties moving in and out of the shelf. The same process was performed on float 6041 but the maximum change in distance

from the linearly interpolated position was 65.7 km (just under 0.6° of latitude), indicating that the linear interpolation was close to the likely float position with relatively small meanders. Therefore, the positions were left as interpolated, and the 6042 profiles will serve as an example. For the purposes of this paper, under ice positions for the winter 2019 profiles were not modified, but a similar process could be applied to both these and future profiles.

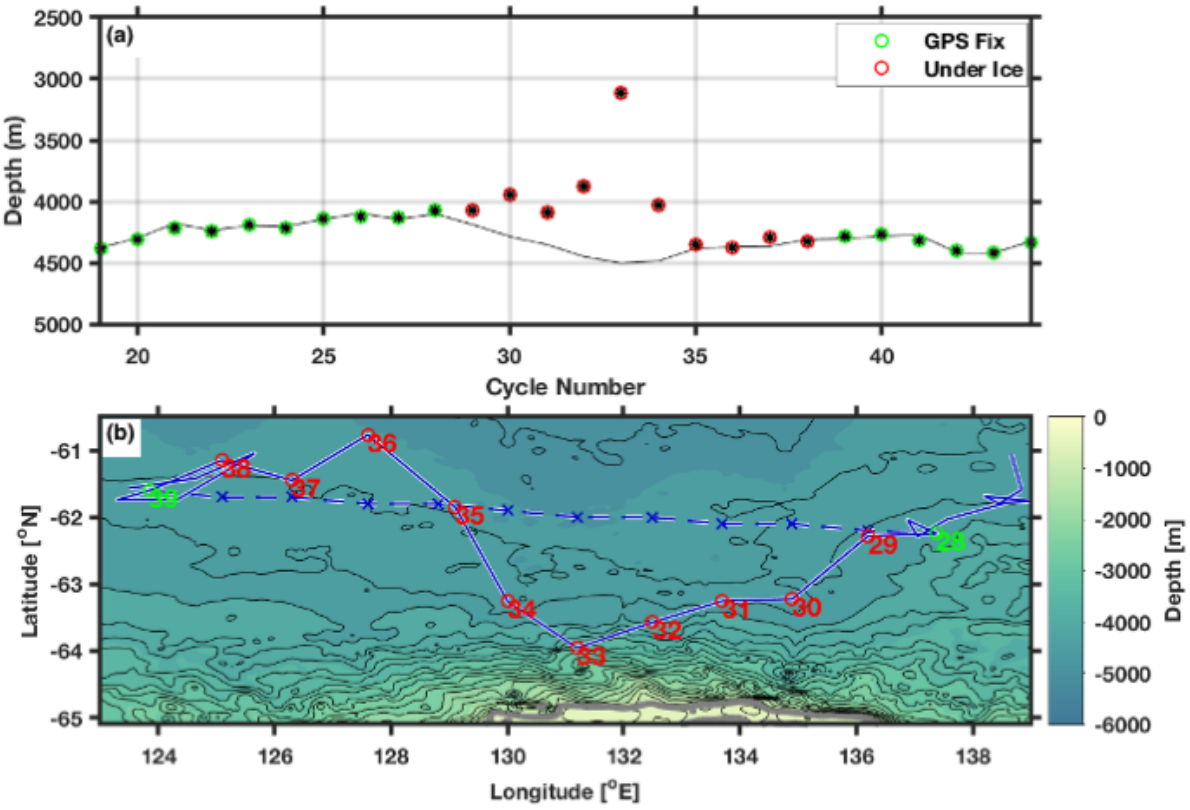

Figure A1: (a) Max depth of each profile (black asterisk) compared to the ETOPO1 bathymetry depth at the interpolated location (black line). Profiles are marked with circles denoting whether they reached the surface to receive a GPS fix (green circle) or were under ice (red circle). (b) Cycles 19-44 of 6042 are shown, with the interpolated (x's, dashed line) and guessed (solid) paths both shown for cycles 29-38. Circles denote the same as in (a). 200 m ETOPO1 bathymetry contours (black) are plotted at the back, with the 500 m isobath (grey) emphasized.

A.2 Deep, Cold Plume Flowing Off-Shelf

The proposed path of float 6042, estimated from the maximum depth measured by the float suggests a drastically different trajectory during the winter of 2018 wherein the float flowed south towards the shelf then quickly off again back into the deeper part of the basin (Figure A1b). The speed and bottom properties observed by the float suggest the float was entrained in a deep bottom water forming plume-driven flow through the marine canyons that run from the shelf to the abyssal plain in this region, consistent with high resolution models that show these dynamics. Here we briefly describe the properties of the observed plume.

To examine the plume further, the float data were linearly interpolated onto a pressure grid from 0-6000 dbar with 10 dbar intervals. The mean bottom conditions in these profiles were defined as the average values recorded from the maximum depth to 200 m above. Comparison of the deep float temperature and salinity profiles to profiles from SR03 at corresponding bathymetric contours confirm that the properties observed by the float align well with the float sampling the colder fresher waters found closer on the Antarctic shelf.

The plume is seen in the float's cycle numbers 31-39, where the mean bottom temperature stays near -0.55°C and the mean bottom salinity stays near 34.651, with slight increases in both further into the basin (Figure A2a,b). The plume, defined as waters colder than -0.5°C, is largest in cycle number 33 on the slope at almost 400 m thick, and it steadily decreases with the offshore movement of the float (Figure A2c). The float moved into the basin quickly, with average velocities of 18.99 cm/s between stations 34 and 35 and almost 17cm/s between 35 and 36 (Figure A1b). The cold, salty plume flowing off the shelf carried a well-mixed bottom layer of anomalous θ-S properties much further north into the basin than usually seen. The

bottom properties, size, and spread of the plume is consistent with deep plumes seen in high resolution models.

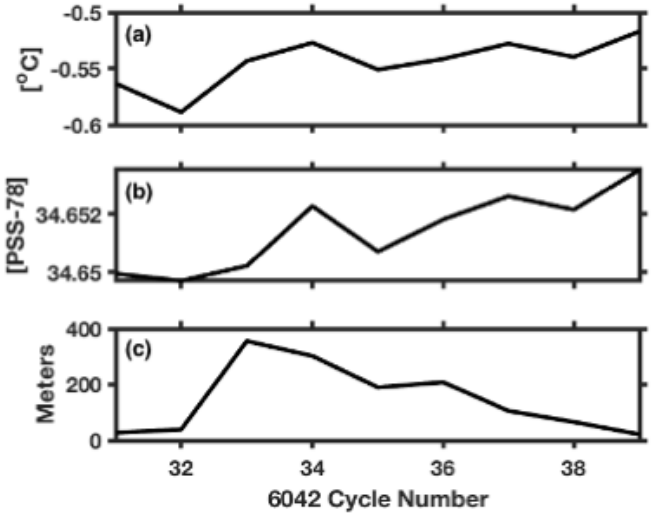

Figure A2: The mean θ (a) and salinity (b) within the deep plume defined as waters between the -0.5°C isotherm and the bottom. (c) The height of the -0.5°C isotherm off the bottom, defined as the maximum depth recorded in the profile.

Bibliography

Aoki, S., S. R. Rintoul, S. Ushio, S. Watanabe, & N. L. Bindoff (2005), Freshening of the Adélie Land Bottom water near 140 E, *Geophys. Res. Lett.*, *32*, L23601, doi:10.1029/2005GL024246.

Aoki, S., Kobayashi, R., Rintoul, S. R., Tamura, T., & Kusahara, K. (2017), Changes in water properties and flow regime on the continental shelf off the Adélie/George V Land coast, East Antarctica, after glacier tongue calving, *J. Geophys. Res. Oceans*, 122, 6277– 6294, doi:10.1002/2017JC012925.

Bindoff, N.L., Rintoul, SR & Massom, RA (2000), Bottom water formation and polynyas in Adelie Land, Antarctica , *Papers and Proceedings of the Royal Society of Tasmania*, vol. 133, no. 3 , pp. 51-56 , doi: 10.26749/rstpp.133.3.51.

Bindoff, N.L., Rosenberg, M. & Warner, M. (2000). On the circulation and water masses over the Antarctic continental slope and rise between 80 and 150°E. Deep Sea Research Part II: Topical Studies in Oceanography. 47. 2299-2326. 10.1016/S0967-0645(00)00038-2.

Boé, J., Hall, A., & Qu, X. (2009), Deep ocean heat uptake as a major source of spread in transient climate change simulations, *Geophys. Res. Lett.*, *36*(22), 2315–5, doi:10.1029/2009GL040845.

Bryan, F. O., Gent, P. R., & Tomas, R. (2014), Can Southern Ocean eddy effects be parameterized in climate models? *J. Clim.*, 27, 411–425, doi:10.1175/jcli-d-12-00759.1.

Castagno, P., Capozzi, V., DiTullio, G. R., Falco, P., Fusco, G., Rintoul, S. R., Spezie, G., & Budillon, G. (2019), Rebound of shelf water salinity in the Ross Sea, *Nature Communications*, 1–6, doi:10.1038/s41467-019-13083-8.

Desbruyères, D. G., Purkey, S. G., McDonagh, E. L., Johnson, G. C., & King, B. A. (2016), Deep and abyssal ocean warming from 35 years of repeat hydrography, *Geophys. Res. Lett.*, *43*(19), 10,356–10,365, doi:10.1002/2016GL070413.

Ganachaud, A., & Wunsch, C. (2000), Improved estimates of global ocean circulation, heat transport and mixing from hydrographic data, *Nature*, *408*(6811), 453–457, doi:10.1038/35044048.

Jacobs, S. S., & Giulivi, C. F. (2010), Large Multidecadal Salinity Trends near the Pacific–Antarctic Continental Margin, *J. Climate*, *23*(17), 4508–4524, doi:10.1175/2010JCLI3284.1.

Jacobs, S. S., Giulivi, C. F., & Mele, P. A. (2002). Freshening of the Ross Sea during the late 20th century. *Science*, *297*(5580), 386-389.

Johnson, G. C. (2008), Quantifying Antarctic Bottom Water and North Atlantic Deep Water volumes, *J. Geophys. Res.*, *113*(C5), C05027–13, doi:10.1029/2007JC004477.

Johnson, G. C., Purkey, S. G., Zilberman, N. V., & Roemmich, D. (2019), Deep Argo Quantifies Bottom Water Warming Rates in the Southwest Pacific Basin, *Geophys. Res. Lett.*, *46*(5), 2662–2669, doi:10.1029/2018GL081685.

Joyce, T. M. (1991). Introduction to the collection of expert reports compiled for the WHP Programme. WOCE Oceanographic Programme Operations and Methods. WOCE Operations Manual. WHP Office Report WHPO-91-1, WOCE Report No. 68/91. 4 pp. https://www.nodc.noaa.gov/woce/woce_v3/wocedata_1/whp/manuals.htm

Klatt, O., Boebel, O., & Fahrbach, E. (2007), A Profiling Float's Sense of Ice, *J. Atmos. Oceanic Technol.*, *24*(7), 1301–1308, doi:10.1175/JTECH2026.1.

Kobayashi, T. (2018), Rapid volume reduction in Antarctic Bottom Water off the Adélie/George V Land coast observed by deep floats, *Deep-Sea Research Part I*, *140*, 95–117, doi:10.1016/j.dsr.2018.07.014.

Kouketsu, S., Doi, T., Igarashi, H., Katsumata, K., Kawai, Y., Kawano, T., Masuda, S., Sasaki, Y., Sugiura, N., Toyoda, T., & Uchida, H. (2011), Deep ocean heat content changes estimated from observation and reanalysis product and their influence on sea level change, *J. Geophys. Res.*, *116*(C3), C03012, doi:10.1029/2010JC006464.

Lumpkin, R., & Speer, K. (2007), Global Ocean Meridional Overturning, *J. Phys. Oceanogr.*, *37*(10), 2550–2562, doi:10.1175/JPO3130.1.

Massom, R. A., Hill, K. L., Lytle, V. I., Worby, A. P., Paget, M. J., & Allison, I. (2001). Effects of regional fast-ice and iceberg distributions on the behaviour of the Mertz Glacier polynya, East Antarctica. *Annals of Glaciology*, *33*, 391-398, doi:10.3189/172756401781818518.

Menezes, V. V., Macdonald, A. M., & Schatzman, C. (2017), Accelerated freshening of Antarctic Bottom Water over the last decade in the Southern Indian Ocean, *Sci. Adv.*, *3*(1), e1601426–10, doi:10.1126/sciadv.1601426.

Murphy, D., & Martini, K. (2018): Determination of conductivity cell compressibility for Argo Program CTDs and MicroCATs. *2018 Ocean Sciences Meeting*, Portland, OR, Amer. Geophys. Union, IS24E-2622.

Newsom, E. R., Abernathey, R., Bitz, C. M., Bryan, F. O., & Gent, P. R. (2016), Southern Ocean Deep Circulation and Heat Uptake in a High-Resolution Climate Model, *J. Climate*, *29*(7), 2597–2619, doi:10.1175/JCLI-D-15-0513.1.

Orsi, A. H., Bullister, J. L., & Johnson, G. C. (1999), Circulation, mixing, and production of Antarctic Bottom Water, *Progress in Oceanography* 43: 55-109, doi:10.1016/S0079-6611(99)00004-X.

Purkey, S. G., & Johnson, G. C. (2010), Warming of global abyssal and deep Southern Ocean waters between the 1990s and 2000s: Contributions to global heat and sea level rise budgets, doi:10.1175/2010JCLI3682.1.

Purkey, S. G., & Johnson, G. C. (2012), Global Contraction of Antarctic Bottom Water between the 1980s and 2000s, *J. Climate*, *25*(17), 5830–5844, doi:10.1175/JCLI-D-11-00612.1.

Purkey, S. G., & Johnson, G. C. (2013), Antarctic Bottom Water Warming and Freshening: Contributions to Sea Level Rise, Ocean Freshwater Budgets, and Global Heat Gain, *J. Climate*, *26*(16), 6105–6122, doi:10.1175/JCLI-D-12-00834.1.

Purkey, S. G., Johnson, G. C., Katsumata, K., Mecking, S., Sloyan, B. M., Smethie, W., Talley, L. D., Wijffels, S. E. (2019), Unabated Bottom Water Warming and Freshening in the South Pacific Ocean, *J. Geophys. Res. Oceans*, *124*(3), 1778–1794, doi:10.1029/2018JC014775.

Rintoul, S. R. (1998), On the origin and influence of Adélie Land Bottom Water, in Ocean, Ice and Atmosphere: Interactions at Antarctic Continental Margin, Antarct. Res. Ser., vol. 75, edited by S. S. Jacobs, and R. Weiss, pp. 151–171, AGU, Washington, D. C., doi:10.1029/AR075p0151.

Rintoul, S. R. (2007), Rapid freshening of Antarctic Bottom Water formed in the Indian and Pacific oceans, doi:10.1029/2006GL028550.

Roemmich, D., Sherman, J. T., Davis, R. E., Grindley, K., McClune, M., Parker, C. J., Black, D.N., Zilberman, N., Purkey, S.G., Sutton, P.J. & Gilson, J. (2019). Deep SOLO: A Full-Depth Profiling Float for the Argo Program. *Journal of Atmospheric and Oceanic Technology*, *36*(10), 1967-1981, doi:10.1175/JTECH-D-19-0066.1.

Scanderbeg, M., King, B., Klein, B., Rannou, J. P., Schmid, C., Van Wijk, E., Wong, A. (2019). Argo DAC profile cookbook. doi:10.13155/41151

Shimada, K., Aoki, S., Ohshima, K. I., & Rintoul, S. R. (2012). Influence of Ross Sea Bottom Water changes on the warming and freshening of the Antarctic Bottom Water in the Australian-Antarctic Basin. *Ocean Science*, *8*(4).

Sloyan, B. M., & Rintoul, S. R. (2001). Circulation, Renewal, and Modification of Antarctic Mode and Intermediate Water. *J. Phys. Oceanogr.*, 31, 1005–1030, https://doi.org/10.1175/1520-0485(2001)031<1005:CRAMOA>2.0.CO;2.

Snow, K., Rintoul, S. R., Sloyan, B. M., & Hogg, A. M. (2018). Change in dense shelf water and Adélie Land bottom water precipitated by iceberg calving. *Geophysical Research Letters*, *45*(5), 2380-2387.

Stewart, A. L., Klocker, A., & Menemenlis, D. (2019). Acceleration and Overturning of the Antarctic Slope Current by Winds, Eddies, and Tides. *J. Phys. Oceanogr.*, **49**, 2043–2074, https://doi.org/10.1175/JPO-D-18-0221.1.

Swift, J., & Orsi, A. H. (2012), Sixty-Four Days of Hydrography and Storms: RVIB Nathaniel B. Palmer's 2011 S04P Cruise, *oceanog*, *25*(3), 54–55, doi:10.5670/oceanog.2012.74.

Talley, L. D. (2003), Shallow, Intermediate, and Deep Overturning Components of the Global Heat Budget, *J. Phys. Oceanogr.*, *33*(3), 530–560, doi:10.1175/1520-0485(2003)033<0530:SIADOC>2.0.CO;2.

Talley, L. D., Feely, R. A., Sloyan, B. M., Wanninkhof, R., Baringer, M. O., Bullister, J. L., Carlson, C.A., Doney, S.C., Fine, R.A., Firing, E. & Gruber, N. (2016). Changes in Ocean Heat, Carbon Content, and Ventilation: A Review of the First Decade of GO-SHIP Global Repeat Hydrography. *Annual Review of Marine Science*, *8*, 185-215. https://doi.org/10.1146/annurev-marine-052915-100829

Tomczak, M., & Large, D. (1989). Optimum Multiparameter Analysis of Mixing in the Thermocline of the Eastern Indian-Ocean, *J. Geophys. Res. Oceans*, *94*(C11), 16141–16149.

van Wijk, E. M., & Rintoul, S. R. (2014). Freshening drives contraction of Antarctic bottom water in the Australian Antarctic Basin. *Geophysical Research Letters*, *41*(5), 1657-1664.

Wallace, L. O., van Wijk, E. M., Rintoul, S. R., & Hally, B. (2020). Bathymetry-constrained navigation of Argo floats under sea ice on the Antarctic continental shelf. *Geophysical Research Letters*, 47, e2020GL087019. https://doi.org/10.1029/2020GL087019

Wendler, G., Stearns, C., Weidner, G., Dargaud, G., & Parish, T. (1997). On the extraordinary katabatic winds of Adélie Land. *Journal of Geophysical Research: Atmospheres*, *102*(D4), 4463-4474.

Williams, G. D., Bindoff, N. L., Marsland, S. J., & Rintoul, S. R. (2008). Formation and export of dense shelf water from the Adélie Depression, East Antarctica, *J. Geophys. Res.*, *113*(C4), L23601–12, doi:10.1029/2007JC004346.